Coexisting polarized four-wave mixing processes in a two-level atomic system

Ruimin Wang,[1,2] Zhenkun Wu,[1] Suling Sang,[1] Jianping Song,[1] Huaibin Zheng,[1] Zhiguo Wang,[1] Changbiao Li,[1] and Yanpeng Zhang[1,3]

[1]*Key Laboratory for Physical Electronics Devices of the Ministry of Education & Shaanxi Key Laboratory of Information Photonic Technique and School of Science, Xi'an Jiaotong University, Xi'an 710049, China*

[2]*e-mail: wangrm@mail.xjtu.edu.cn*

[3]*e-mail: ypzhang@mail.xjtu.edu.cn*

Received June 13, 2011; revised September 1, 2011; accepted October 3, 2011; posted October 11, 2011 (Doc. ID 149176); published November 18, 2011

We investigate the polarization dependence of eight coexisting four-wave mixing (FWM) signals in a two-level atomic system. The intensities and polarization states of coexisting FWM signals are modulated by the polarization configurations and frequency detunings of the incident fields. The suppression and enhancement due to the dressing effects present different polarization dependences. Both the mutual-dressing effect and the self-dressing effect are considered to explain the observed phenomena.

OCIS codes: 190.4380, 270.4180, 300.2570, 320.7110, 030.1670.

1. INTRODUCTION

Four-wave mixing (FWM) is a powerful technique for generating coherent radiation and studying a variety of coherent optical phenomena. In recent years, FWM has been widely used to observe atomic coherence [1,2], generate entangled photon pairs [3,4], and to coherently control field–matter interactions [5]. In these processes, the intensities of the FWM signals are related to the polarizations of the incident lasers. That is because the variation of the incidence polarization leads to different transition pathways among degenerate Zeeman sublevels. Different transitions generally have different coupling strength values, which are indicated by Clebsch–Gordan (CG) coefficients, and different FWM transition pathways are dressed by different dressing fields. So we can coherently control the nonlinear signal by suitably designing the polarizations of the incident laser beams.

The polarization properties of two-photon resonant FWM have been well investigated previously [6–9]. Recently, we studied the polarization dependences of FWM and dressing effects in two-level and cascaded three-level atomic systems [10], as well as the multiwave mixing processes in a reversed-Y-type system with electromagnetically induced transparency windows at different polarization configurations [11]. In this paper, the polarization properties of several coexisting FWM signals in a two-level system are investigated. In the presence of additional coupling laser fields, more FWM processes can coexist in the same system. In this case, several interesting physical phenomena can occur, such as quantum interference, competition, and mutual dressing among these FWM signals. We observe the intensities and polarizations of these coexisting FWM signals under different polarization configurations and different frequency detunings of the incident fields. Moreover, the polarization dependence of mutual-dressing effect and the interaction among coexisting FWM signals are investigated. These results verify that the coexisting FWM processes can be modulated via the polarization configurations and frequency detunings of the incident fields. Such controlled FWM signals are important for optical communication and quantum information processes.

2. EXPERIMENT SETUP

The experiments are carried out in a Na atom vapor oven (the sodium atomic density is about $1.5\times10^{13}\,\mathrm{cm}^{-3}$, $T=235\,°\mathrm{C}$). As shown in Fig. 1(b), energy levels $|a\rangle(3S_{1/2})$ and $|b\rangle(3P_{3/2})$ form a two-level atomic system, the resonant frequency of which is ω_0. Six laser beams are all driving the transition between $|a\rangle$ and $|b\rangle$. Two laser beams E_c (ω_c, $\mathbf{k}_c$, Rabi frequency G_c, and intensity $I=4.4\,\mathrm{W/cm^2}$) and E'_c (ω_c, $\mathbf{k}'_c$, G'_c, and $4.4\,\mathrm{W/cm^2}$) propagate in the opposite direction of the weak probe beam E_p (ω_p, $\mathbf{k}_p$, G_p, and $0.3\,\mathrm{W/cm^2}$). These three laser beams come from the same dye laser DL1 (10 Hz repetition rate, 5 ns pulse width, and $0.04\,\mathrm{cm}^{-1}$ linewidth) with a frequency detuning $\Delta_1=\omega_0-\omega_c$, pumped by the second-harmonic beam of a Nd:YAG laser. The other three laser beams E_d (ω_d, $\mathbf{k}_d$, G_d, and $3.2\,\mathrm{W/cm^2}$), E'_d (ω_d, $\mathbf{k}'_d$, G'_d, and $3.2\,\mathrm{W/cm^2}$), and E'_p (ω'_p, $\mathbf{k}'_p$, G'_p, $0.2\,\mathrm{W/cm^2}$) are from another dye laser DL2 (which has the same characteristics as DL1) with a frequency detuning $\Delta_2=\omega_0-\omega_d$. In this case, there are eight FWM signals coexisting in one atomic system. The phase-matching conditions and frequencies of generated FWM signals are tabulated in Table 1. These FWM signals propagate in two directions (FWM signals $\mathbf{k}_{s1}$, $\mathbf{k}_{s2}$, $\mathbf{k}_{s3}$, and $\mathbf{k}_{s4}$ propagate in the opposite direction of $\mathbf{k}'_c$. FWM signals $\mathbf{k}_{s5}$, $\mathbf{k}_{s6}$, $\mathbf{k}_{s7}$, and $\mathbf{k}_{s8}$ propagate in the opposite direction of $\mathbf{k}'_d$). All the FWM signals are first split into two equal components by a splitter, in which one is detected directly (denoted as I_T), and the other is decomposed into P- and S-polarized components by a polarization beam splitter (PBS). Two photomultiplier tube (PMT) detectors are used to receive the P or S component of these FWM signals in the opposite direction of $\mathbf{k}'_c$ (PMT1) and $\mathbf{k}'_d$ (PMT2), respectively. A half-wave plate (HWP) and a quarter-wave plate (QWP) are selectively used (in different experiments) to control the polarization states of the incident fields.

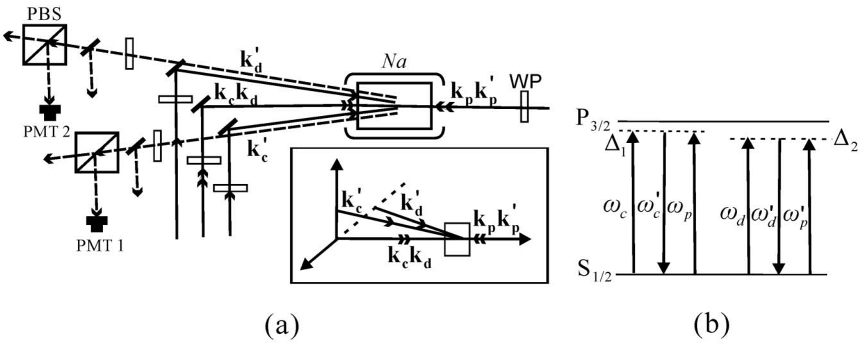

Fig. 1. Schematic diagrams of the experimental setup and the relevant energy levels in Na atom.

3. THEORETICAL MODEL

When six laser beams are all turned on, there are eight FWM signals coexisting in one atomic system. The quantum constructive or destructive interference between different pathways can result in the mutual-dressing effect between these coexisting FWM signals. Because of the application of several wave plates to modify the polarization states of the incident fields, Zeeman sublevels of each involved energy level will play an important role in the interaction between atoms and polarized fields. So we theoretically investigate the generated FWM signals by considering the generation process among various Zeeman sublevels in the semiclassical framework. The transition pathways of generated FWM are presented in Fig. 2. It is based on the fact that different polarization schemes can excite different transition pathways in the Zeeman-degenerate atomic systems. As a sample, Table 2 lists all the perturbation chains of the FWM signals when fields $\mathbf{k}_c$ and $\mathbf{k}_c'$ are changed by the QWP. The total FWM signal can be considered as the summed contribution of each perturbation chain. According to the experimental setup, the x axis is the original polarization direction of all the incident fields, and it is also the quantization axis. We then decompose an arbitrary field into two components: parallel to and perpendicular to the x axis, respectively. When this field interacts with a two-level atom, the perpendicular component can be decomposed into equally left-circularly and right-circularly polarized components. The generated FWM signals contain linearly polarized component I_L and circularly polarized component I_C. We have $I_P = I_L \sin^2\alpha + I_C/2$, where α is the angle between the P polarization and the polarization of the linearly polarized signal, $I_S = I_L \cos^2\alpha + I_C/2$, and $I_T = I_S + I_P = I_L + I_C$ [12].

Using the method of a perturbation chain [13–15], we can obtain the expressions of various density matrix elements corresponding to the third-order nonlinear susceptibilities under different polarization schemes. When the polarizations of $\mathbf{k}_c$ and $\mathbf{k}_c'$ are changed by QWP, the corresponding density matrix elements of undressed-FWM signals in P and S polarization are

Table 1. Wave Vectors and Frequencies of the Generated FWM Signals Detected by PMT1 and PMT2

	Wave Vectors	Frequencies
PMT1	$\mathbf{k}_{s1} = \mathbf{k}_p + \mathbf{k}_c - \mathbf{k}_c'$	$\omega_{s1} = \omega_c$
	$\mathbf{k}_{s2} = \mathbf{k}_p + \mathbf{k}_d - \mathbf{k}_c'$	$\omega_{s2} = \omega_d$
	$\mathbf{k}_{s3} = \mathbf{k}_p' + \mathbf{k}_c - \mathbf{k}_c'$	$\omega_{s3} = \omega_d$
	$\mathbf{k}_{s4} = \mathbf{k}_p' + \mathbf{k}_d - \mathbf{k}_c'$	$\omega_{s4} = 2\omega_d - \omega_c$
PMT2	$\mathbf{k}_{s5} = \mathbf{k}_p' + \mathbf{k}_d - \mathbf{k}_d'$	$\omega_{s5} = \omega_d$
	$\mathbf{k}_{s6} = \mathbf{k}_p' + \mathbf{k}_c - \mathbf{k}_d'$	$\omega_{s6} = \omega_c$
	$\mathbf{k}_{s7} = \mathbf{k}_p + \mathbf{k}_d - \mathbf{k}_d'$	$\omega_{s7} = \omega_c$
	$\mathbf{k}_{s8} = \mathbf{k}_p + \mathbf{k}_c - \mathbf{k}_d'$	$\omega_{s8} = 2\omega_c - \omega_d$

$$\rho^{k_1,k_1'}_{P(\mathrm{PMT1})} = -i\sum_{M=\pm1/2}\left[\frac{|G^0_{c_M}|^2}{\Gamma_{a_Ma_M}d_1}\left(\frac{G^0_{p_M}}{d_1}+\frac{G'^0_{p_M}}{d_2}\right) + \frac{(G^0_{c_M})^*G^0_{d_M}}{d_3d_2}\left(\frac{G^0_{p_M}}{d_2}+\frac{G'^0_{p_M}}{d_4}\right)\right] - i\sum_{M=\pm1/2}\frac{1}{\Gamma_{a_Ma_M}}\left(\frac{(G^-_{c_M})^*G^-_{c_M}}{d_{11}}+\frac{(G^+_{c_M})^*G^+_{c_M}}{d_{12}}\right) \times\left(\frac{G^0_{p_M}}{d_1}+\frac{G'^0_{p_M}}{d_2}\right), \tag{1}$$

$$\rho^{k_1,k_1'}_{s(\mathrm{PMT1})} = -i\sum_{M=\pm1/2}\left[\frac{G^0_{c_M}(G'^{\pm}_{c_M})^*}{\Gamma_{a_Ma_{-M}}d_1}\left(\frac{G'^0_{p_M}}{d_{14}}+\frac{G^0_{p_M}}{d_{13}}\right) + \frac{G^0_{d_M}(G'^{\pm}_{c_M})^*}{d_7d_2}\left(\frac{G^0_{p_M}}{d_{14}}+\frac{G'^0_{p_M}}{d_8}\right)\right], \tag{2}$$

$$\rho^{k_1,k_1'}_{P(\mathrm{PMT2})} = -i\sum_{M=\pm1/2}\left[\frac{|G^0_{d_M}|^2}{\Gamma_{a_Ma_M}d_2}\left(\frac{G^0_{p_M}}{d_1}+\frac{G'^0_{p_M}}{d_2}\right) + \frac{G^0_{c_M}(G^0_{d_M})^*}{d_5d_1}\left(\frac{G^0_{p_M}}{d_6}+\frac{G'^0_{p_M}}{d_1}\right)\right], \tag{3}$$

$$\rho^{k_1,k_1'}_{s(\mathrm{PMT2})} = -i\sum_{M=\pm1/2}\left[\frac{G^{\mp}_{c_M}(G'^0_{c_M})^*}{\Gamma_{a_Ma_{-M}}d_{13}}\left(\frac{G^0_{p_M}}{d_{13}}+\frac{G'^0_{p_M}}{d_{14}}\right) + \frac{G^{\mp}_{c_M}(G'^0_{d_M})^*}{d_9d_{13}}\left(\frac{G^0_{p_M}}{d_{10}}+\frac{G'^0_{p_M}}{d_{13}}\right)\right], \tag{4}$$

where $G_i = -\mu_i E_i/\hbar$ ($i = c,\ d,\ p$) is the Rabi frequency; $d_1 = i\Delta_1 + \Gamma_{b_Ma_M}$, $d_2 = i\Delta_2 + \Gamma_{b_Ma_M}$, $d_3 = i(\Delta_2 - \Delta_1) + \Gamma_{a_Ma_M}$, $d_4 = i(2\Delta_2 - \Delta_1) + \Gamma_{b_Ma_M}$, $d_5 = i(\Delta_1 - \Delta_2) + \Gamma_{a_Ma_M}$, $d_6 = i(2\Delta_1 - \Delta_2) + \Gamma_{b_Ma_M}$, $d_7 = i(\Delta_2 - \Delta_1) + \Gamma_{a_Ma_{-M}}$, $d_8 = i(2\Delta_2 - \Delta_1) + \Gamma_{b_{-M}a_M}$, $d_9 = \Gamma_{a_Ma_{-M}} + i(\Delta_1 - \Delta_2)$, $d_{10} = i(2\Delta_1 - \Delta_2) + \Gamma_{b_{-M}a_M}$, $d_{11} = i\Delta_1 + \Gamma_{b_{M-1}a_M}$, $d_{12} = i\Delta_1 + \Gamma_{b_{M+1}a_M}$, $d_{13} = i\Delta_1 + \Gamma_{b_{-M}a_M}$, $d_{14} = i\Delta_2 + \Gamma_{b_{-M}a_M}$; and Γ_{ab} and Γ_{ba} are the transverse relaxation rates and Γ_{aa} is the longitudinal one.

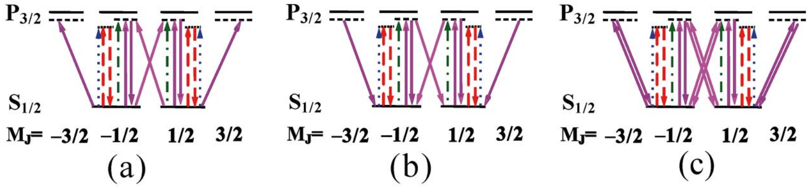

Fig. 2. (Color online) Schematic of two-level system configuration consisting of Zeeman sublevels. (a) QWP changes field $\mathbf{k}_c$, (b) QWP changes field $\mathbf{k}_c'$, (c) QWP changes both fields $\mathbf{k}_c$ and $\mathbf{k}_c'$. Solid lines, the coupling fields $\mathbf{k}_c$ and $\mathbf{k}_c'$; dashed lines, coupling fields $\mathbf{k}_d$ and $\mathbf{k}_d'$; dashed–dotted lines, probe field $\mathbf{k}_p$; dotted lines, probe field $\mathbf{k}_p'$.

Now we consider only the mutual-dressing effect of coexisting FWM signals. As Fig. 2 shows, different channels have different dressing strengths. When the rotation angle of the QWP is at 0°, only the transition pathways $|a_{-1/2}\rangle \cdots |b_{-1/2}\rangle$ and $|a_{1/2}\rangle \cdots |b_{1/2}\rangle$ are allowed. In this case, the density matrix elements of the dressing FWM signals in P polarization are

Table 2. Perturbation Chains of Horizontally Polarized Components of FWM Signals When Fields $\mathbf{k}_c$ and $\mathbf{k}_c'$ are Changed by the QWP

Subsystem generating P-polarization signal	$|a_{-1/2}\rangle \xrightarrow{G_{c1}^{-}} |b_{-3/2}\rangle \xrightarrow{(G_{c1}^{\prime -})^{*}} |a_{-1/2}\rangle \xrightarrow{G_{p1}^{0}} |b_{-1/2}\rangle \xrightarrow{(G_{F1}^{0})^{*}} |a_{-1/2}\rangle : \mathbf{k}_c - \mathbf{k}_c' + \mathbf{k}_p$
	$|a_{-1/2}\rangle \xrightarrow{G_{c1}^{-}} |b_{-3/2}\rangle \xrightarrow{(G_{c1}^{\prime -})^{*}} |a_{-1/2}\rangle \xrightarrow{G_{p1}^{\prime 0}} |b_{-1/2}\rangle \xrightarrow{(G_{F1}^{0})^{*}} |a_{-1/2}\rangle : \mathbf{k}_c - \mathbf{k}_c' + \mathbf{k}_p'$
	$|a_{-1/2}\rangle \xrightarrow{G_{c1}^{0}} |b_{-1/2}\rangle \xrightarrow{G_{c1}^{\prime 0}} |a_{-1/2}\rangle \xrightarrow{G_{p1}^{0}} |b_{-1/2}\rangle \xrightarrow{(G_{F1}^{0})^{*}} |a_{-1/2}\rangle : \mathbf{k}_c - \mathbf{k}_c' + \mathbf{k}_p$
	$|a_{-1/2}\rangle \xrightarrow{G_{c1}^{0}} |b_{-1/2}\rangle \xrightarrow{G_{c1}^{\prime 0}} |a_{-1/2}\rangle \xrightarrow{G_{p1}^{\prime 0}} |b_{-1/2}\rangle \xrightarrow{(G_{F1}^{0})^{*}} |a_{-1/2}\rangle : \mathbf{k}_c - \mathbf{k}_c' + \mathbf{k}_p'$
	$|a_{-1/2}\rangle \xrightarrow{G_{c1}^{0}} |b_{-1/2}\rangle \xrightarrow{G_{d1}^{\prime 0}} |a_{-1/2}\rangle \xrightarrow{G_{p1}^{0}} |b_{-1/2}\rangle \xrightarrow{(G_{F1}^{0})^{*}} |a_{-1/2}\rangle : \mathbf{k}_c - \mathbf{k}_d' + \mathbf{k}_p$
	$|a_{-1/2}\rangle \xrightarrow{G_{c1}^{0}} |b_{-1/2}\rangle \xrightarrow{G_{d1}^{\prime 0}} |a_{-1/2}\rangle \xrightarrow{G_{p1}^{\prime 0}} |b_{-1/2}\rangle \xrightarrow{(G_{F1}^{0})^{*}} |a_{-1/2}\rangle : \mathbf{k}_c - \mathbf{k}_d' + \mathbf{k}_p'$
	$|a_{-1/2}\rangle \xrightarrow{G_{c1}^{+}} |b_{1/2}\rangle \xrightarrow{(G_{c1}^{\prime +})^{*}} |a_{-1/2}\rangle \xrightarrow{G_{p2}^{0}} |b_{-1/2}\rangle \xrightarrow{(G_{F2}^{0})^{*}} |a_{-1/2}\rangle : \mathbf{k}_c - \mathbf{k}_c' + \mathbf{k}_p$
	$|a_{-1/2}\rangle \xrightarrow{G_{c1}^{+}} |b_{1/2}\rangle \xrightarrow{(G_{c1}^{\prime +})^{*}} |a_{-1/2}\rangle \xrightarrow{G_{p2}^{\prime 0}} |b_{-1/2}\rangle \xrightarrow{(G_{F2}^{0})^{*}} |a_{-1/2}\rangle : \mathbf{k}_c - \mathbf{k}_c' + \mathbf{k}_p'$
	$|a_{-1/2}\rangle \xrightarrow{G_{d1}^{0}} |b_{-1/2}\rangle \xrightarrow{G_{c1}^{\prime 0}} |a_{-1/2}\rangle \xrightarrow{G_{p1}^{0}} |b_{-1/2}\rangle \xrightarrow{(G_{F1}^{0})^{*}} |a_{-1/2}\rangle : \mathbf{k}_d - \mathbf{k}_c' + \mathbf{k}_p$
	$|a_{-1/2}\rangle \xrightarrow{G_{d1}^{0}} |b_{-1/2}\rangle \xrightarrow{G_{c1}^{\prime 0}} |a_{-1/2}\rangle \xrightarrow{G_{p1}^{\prime 0}} |b_{-1/2}\rangle \xrightarrow{(G_{F1}^{0})^{*}} |a_{-1/2}\rangle : \mathbf{k}_d - \mathbf{k}_c' + \mathbf{k}_p'$
	$|a_{-1/2}\rangle \xrightarrow{G_{d1}^{0}} |b_{-1/2}\rangle \xrightarrow{G_{d1}^{\prime 0}} |a_{-1/2}\rangle \xrightarrow{G_{p1}^{0}} |b_{-1/2}\rangle \xrightarrow{(G_{F1}^{0})^{*}} |a_{-1/2}\rangle : \mathbf{k}_d - \mathbf{k}_d' + \mathbf{k}_p$
	$|a_{-1/2}\rangle \xrightarrow{G_{d1}^{0}} |b_{-1/2}\rangle \xrightarrow{G_{d1}^{\prime 0}} |a_{-1/2}\rangle \xrightarrow{G_{p1}^{\prime 0}} |b_{-1/2}\rangle \xrightarrow{(G_{F1}^{0})^{*}} |a_{-1/2}\rangle : \mathbf{k}_d - \mathbf{k}_d' + \mathbf{k}_p'$
	$|a_{1/2}\rangle \xrightarrow{G_{c2}^{-}} |b_{-1/2}\rangle \xrightarrow{(G_{c2}^{\prime -})^{*}} |a_{1/2}\rangle \xrightarrow{G_{p2}^{0}} |b_{1/2}\rangle \xrightarrow{(G_{F2}^{0})^{*}} |a_{1/2}\rangle : \mathbf{k}_c - k_c' + \mathbf{k}_p$
	$|a_{1/2}\rangle \xrightarrow{G_{c2}^{-}} |b_{-1/2}\rangle \xrightarrow{(G_{c2}^{\prime -})^{*}} |a_{1/2}\rangle \xrightarrow{G_{p2}^{\prime 0}} |b_{1/2}\rangle \xrightarrow{(G_{F2}^{0})^{*}} |a_{1/2}\rangle : \mathbf{k}_c - \mathbf{k}_c' + \mathbf{k}_p'$
	$|a_{1/2}\rangle \xrightarrow{G_{c2}^{0}} |b_{1/2}\rangle \xrightarrow{G_{c2}^{\prime 0}} |a_{1/2}\rangle \xrightarrow{G_{p2}^{0}} |b_{1/2}\rangle \xrightarrow{(G_{F2}^{0})^{*}} |a_{1/2}\rangle : \mathbf{k}_c - k_c' + \mathbf{k}_p$
	$|a_{1/2}\rangle \xrightarrow{G_{c2}^{0}} |b_{1/2}\rangle \xrightarrow{G_{c2}^{\prime 0}} |a_{1/2}\rangle \xrightarrow{G_{p2}^{\prime 0}} |b_{1/2}\rangle \xrightarrow{(G_{F2}^{0})^{*}} |a_{1/2}\rangle : \mathbf{k}_c - k_c' + k_p'$
	$|a_{1/2}\rangle \xrightarrow{G_{c2}^{0}} |b_{1/2}\rangle \xrightarrow{G_{d2}^{\prime 0}} |a_{1/2}\rangle \xrightarrow{G_{p2}^{0}} |b_{1/2}\rangle \xrightarrow{(G_{F2}^{0})^{*}} |a_{1/2}\rangle : \mathbf{k}_c - k_d' + \mathbf{k}_p$
	$|a_{1/2}\rangle \xrightarrow{G_{c2}^{0}} |b_{1/2}\rangle \xrightarrow{G_{d2}^{\prime 0}} |a_{1/2}\rangle \xrightarrow{G_{p2}^{\prime 0}} |b_{1/2}\rangle \xrightarrow{(G_{F2}^{0})^{*}} |a_{1/2}\rangle : \mathbf{k}_c - k_d' + k_p'$
	$|a_{1/2}\rangle \xrightarrow{G_{c2}^{+}} |b_{3/2}\rangle \xrightarrow{(G_{c2}^{\prime +})^{*}} |a_{1/2}\rangle \xrightarrow{G_{p2}^{0}} |b_{1/2}\rangle \xrightarrow{(G_{F2}^{0})^{*}} |a_{1/2}\rangle : \mathbf{k}_c - k_c' + \mathbf{k}_p$
	$|a_{1/2}\rangle \xrightarrow{G_{c2}^{+}} |b_{3/2}\rangle \xrightarrow{(G_{c2}^{\prime +})^{*}} |a_{1/2}\rangle \xrightarrow{G_{p2}^{\prime 0}} |b_{1/2}\rangle \xrightarrow{(G_{F2}^{0})^{*}} |a_{1/2}\rangle : \mathbf{k}_c - k_c' + k_p'$
	$|a_{1/2}\rangle \xrightarrow{G_{d2}^{0}} |b_{1/2}\rangle \xrightarrow{G_{c2}^{\prime 0}} |a_{1/2}\rangle \xrightarrow{G_{p2}^{0}} |b_{1/2}\rangle \xrightarrow{(G_{F2}^{0})^{*}} |a_{1/2}\rangle : \mathbf{k}_d - k_c' + \mathbf{k}_p$
	$|a_{1/2}\rangle \xrightarrow{G_{d2}^{0}} |b_{1/2}\rangle \xrightarrow{G_{c2}^{\prime 0}} |a_{1/2}\rangle \xrightarrow{G_{p2}^{\prime 0}} |b_{1/2}\rangle \xrightarrow{(G_{F2}^{0})^{*}} |a_{1/2}\rangle : \mathbf{k}_d - \mathbf{k}_c' + \mathbf{k}_p'$
	$|a_{1/2}\rangle \xrightarrow{G_{d2}^{0}} |b_{1/2}\rangle \xrightarrow{G_{d2}^{\prime 0}} |a_{1/2}\rangle \xrightarrow{G_{p2}^{0}} |b_{1/2}\rangle \xrightarrow{(G_{F2}^{0})^{*}} |a_{1/2}\rangle : \mathbf{k}_d - k_d' + \mathbf{k}_p$
	$|a_{1/2}\rangle \xrightarrow{G_{d2}^{0}} |b_{1/2}\rangle \xrightarrow{G_{d2}^{\prime 0}} |a_{1/2}\rangle \xrightarrow{G_{p2}^{\prime 0}} |b_{1/2}\rangle \xrightarrow{(G_{F2}^{0})^{*}} |a_{1/2}\rangle : \mathbf{k}_d - k_d' + k_p'$
Subsystem generating S-polarization signal	$|a_{-1/2}\rangle \xrightarrow{G_{c1}^{0}} |b_{-1/2}\rangle \xrightarrow{G_{c1}^{\prime -}} |a_{1/2}\rangle \xrightarrow{G_{p1}^{0}} |b_{1/2}\rangle \xrightarrow{(G_{F2}^{+})^{*}} |a_{-1/2}\rangle : \mathbf{k}_c - \mathbf{k}_c' + \mathbf{k}_p$
	$|a_{-1/2}\rangle \xrightarrow{G_{c1}^{0}} |b_{-1/2}\rangle \xrightarrow{G_{c1}^{\prime -}} |a_{1/2}\rangle \xrightarrow{G_{p1}^{\prime 0}} |b_{1/2}\rangle \xrightarrow{(G_{F2}^{+})^{*}} |a_{-1/2}\rangle : \mathbf{k}_c - \mathbf{k}_c' + \mathbf{k}_p'$
	$|a_{-1/2}\rangle \xrightarrow{G_{c1}^{+}} |b_{1/2}\rangle \xrightarrow{G_{c2}^{\prime 0}} |a_{1/2}\rangle \xrightarrow{G_{p2}^{0}} |b_{1/2}\rangle \xrightarrow{(G_{F2}^{+})^{*}} |a_{-1/2}\rangle : \mathbf{k}_c - \mathbf{k}_c' + \mathbf{k}_p$
	$|a_{-1/2}\rangle \xrightarrow{G_{c1}^{+}} |b_{1/2}\rangle \xrightarrow{G_{c2}^{\prime 0}} |a_{1/2}\rangle \xrightarrow{G_{p2}^{\prime 0}} |b_{1/2}\rangle \xrightarrow{(G_{F2}^{+})^{*}} |a_{-1/2}\rangle : \mathbf{k}_c - \mathbf{k}_c' + \mathbf{k}_p'$
	$|a_{-1/2}\rangle \xrightarrow{G_{c1}^{+}} |b_{1/2}\rangle \xrightarrow{G_{d2}^{\prime 0}} |a_{1/2}\rangle \xrightarrow{G_{p2}^{0}} |b_{1/2}\rangle \xrightarrow{(G_{F2}^{+})^{*}} |a_{-1/2}\rangle : \mathbf{k}_c - \mathbf{k}_d' + \mathbf{k}_p$
	$|a_{-1/2}\rangle \xrightarrow{G_{c1}^{+}} |b_{1/2}\rangle \xrightarrow{G_{d2}^{\prime 0}} |a_{1/2}\rangle \xrightarrow{G_{p2}^{\prime 0}} |b_{1/2}\rangle \xrightarrow{(G_{F2}^{+})^{*}} |a_{-1/2}\rangle : \mathbf{k}_c - \mathbf{k}_d' + \mathbf{k}_p'$
	$|a_{-1/2}\rangle \xrightarrow{G_{d1}^{0}} |b_{-1/2}\rangle \xrightarrow{G_{c1}^{\prime -}} |a_{1/2}\rangle \xrightarrow{G_{p2}^{0}} |b_{1/2}\rangle \xrightarrow{(G_{F2}^{+})^{*}} |a_{-1/2}\rangle : \mathbf{k}_d - \mathbf{k}_c' + \mathbf{k}_p$
	$|a_{-1/2}\rangle \xrightarrow{G_{d1}^{0}} |b_{-1/2}\rangle \xrightarrow{G_{c1}^{\prime -}} |a_{1/2}\rangle \xrightarrow{G_{p2}^{\prime 0}} |b_{1/2}\rangle \xrightarrow{(G_{F2}^{+})^{*}} |a_{-1/2}\rangle : \mathbf{k}_d - \mathbf{k}_c' + \mathbf{k}_p'$
	$|a_{1/2}\rangle \xrightarrow{G_{c2}^{-}} |b_{-1/2}\rangle \xrightarrow{G_{c1}^{\prime 0}} |a_{-1/2}\rangle \xrightarrow{G_{p1}^{0}} |b_{-1/2}\rangle \xrightarrow{(G_{F2}^{+})^{*}} |a_{1/2}\rangle : \mathbf{k}_c - \mathbf{k}_c' + \mathbf{k}_p$
	$|a_{1/2}\rangle \xrightarrow{G_{c2}^{-}} |b_{-1/2}\rangle \xrightarrow{G_{c1}^{\prime 0}} |a_{-1/2}\rangle \xrightarrow{G_{p1}^{\prime 0}} |b_{-1/2}\rangle \xrightarrow{(G_{F2}^{+})^{*}} |a_{1/2}\rangle : \mathbf{k}_c - \mathbf{k}_c' + \mathbf{k}_p'$
	$|a_{1/2}\rangle \xrightarrow{G_{c2}^{-}} |b_{-1/2}\rangle \xrightarrow{G_{d1}^{\prime 0}} |a_{-1/2}\rangle \xrightarrow{G_{p1}^{0}} |b_{-1/2}\rangle \xrightarrow{(G_{F2}^{+})^{*}} |a_{1/2}\rangle : \mathbf{k}_c - \mathbf{k}_d' + \mathbf{k}_p$
	$|a_{1/2}\rangle \xrightarrow{G_{c2}^{-}} |b_{-1/2}\rangle \xrightarrow{G_{d1}^{\prime 0}} |a_{-1/2}\rangle \xrightarrow{G_{p1}^{\prime 0}} |b_{-1/2}\rangle \xrightarrow{(G_{F2}^{+})^{*}} |a_{1/2}\rangle : \mathbf{k}_c - \mathbf{k}_d' + \mathbf{k}_p'$
	$|a_{1/2}\rangle \xrightarrow{G_{c2}^{0}} |b_{1/2}\rangle \xrightarrow{G_{c1}^{\prime +}} |a_{-1/2}\rangle \xrightarrow{G_{p1}^{0}} |b_{-1/2}\rangle \xrightarrow{(G_{F2}^{+})^{*}} |a_{1/2}\rangle : \mathbf{k}_c - \mathbf{k}_c' + \mathbf{k}_p$
	$|a_{1/2}\rangle \xrightarrow{G_{c2}^{0}} |b_{1/2}\rangle \xrightarrow{G_{c1}^{\prime +}} |a_{-1/2}\rangle \xrightarrow{G_{p1}^{\prime 0}} |b_{-1/2}\rangle \xrightarrow{(G_{F2}^{+})^{*}} |a_{1/2}\rangle : \mathbf{k}_c - k_c' + k_p'$
	$|a_{1/2}\rangle \xrightarrow{G_{d2}^{0}} |b_{1/2}\rangle \xrightarrow{G_{c1}^{\prime +}} |a_{-1/2}\rangle \xrightarrow{G_{p1}^{0}} |b_{-1/2}\rangle \xrightarrow{(G_{F2}^{+})^{*}} |a_{1/2}\rangle : \mathbf{k}_d - \mathbf{k}_c' + \mathbf{k}_p$
	$|a_{1/2}\rangle \xrightarrow{G_{d2}^{0}} |b_{1/2}\rangle \xrightarrow{G_{c1}^{\prime +}} |a_{-1/2}\rangle \xrightarrow{G_{p1}^{\prime 0}} |b_{-1/2}\rangle \xrightarrow{(G_{F2}^{+})^{*}} |a_{1/2}\rangle : \mathbf{k}_d - \mathbf{k}_c' + \mathbf{k}_p'$

$$\rho_{P(\mathrm{PMT1})}^{k_1,k_1'} = -i\sum_{M=\pm 1/2}\left[\frac{|G^0_{c_M}|^2}{\Gamma_{a_M a_M}\left(d_1+\frac{|G^0_{d_M}|^2}{d_3}\right)}\left(\frac{G^0_{p_M}}{d_1}+\frac{G'^0_{p_M}}{d_2}\right) + \frac{(G^0_{c_M})^* G^0_{d_M}}{d_3\left(d_2+\frac{|(G^0_{d_M})^*|^2}{\Gamma_{a_M a_M}}+\frac{|G^0_{c_M}|^2}{d_5}\right)}\left(\frac{G^0_{p_M}}{d_2}+\frac{G'^0_{p_M}}{d_4}\right)\right], \quad (5)$$

$$\rho_{P(\mathrm{PMT2})}^{k_1,k_1'} = -i\sum_{M=\pm 1/2}\left[\frac{|G^0_{d_M}|^2}{\Gamma_{a_M a_M}\left(d_2+\frac{|G^0_{c_M}|^2}{d_5}\right)}\left(\frac{G^0_{p_M}}{d_1}+\frac{G'^0_{p_M}}{d_2}\right) + \frac{G^0_{c_M}(G^0_{d_M})^*}{d_5\left(d_1+\frac{|(G^0_{c_M})^*|^2}{\Gamma_{a_M a_M}}+\frac{|G^0_{d_M}|^2}{d_5}\right)}\left(\frac{G^0_{p_M}}{d_6}+\frac{G'^0_{p_M}}{d_1}\right)\right]. \quad (6)$$

When the rotation angle of the QWP is at 45°, the incident fields can be decomposed into three components with linear, left-circular, and right-circular polarizations. As shown in Fig. 2, there are six considerable transition pathways in this system: $|a_{-1/2}\rangle\cdots|b_{-3/2}\rangle$, $|a_{-1/2}\rangle\cdots|b_{-1/2}\rangle$, $|a_{-1/2}\rangle\cdots|b_{1/2}\rangle$, $|a_{1/2}\rangle\cdots|b_{-1/2}\rangle$, $|a_{1/2}\rangle\cdots|b_{1/2}\rangle$, and $|a_{1/2}\rangle\cdots|b_{3/2}\rangle$. Each transition pathway corresponds to a different dressing field, and the density matrix elements of the dressing FWM signals in P polarization can be expressed as

$$\begin{aligned}\rho_{P(\mathrm{PMT1})}^{k_1,k_1'} = &-i\sum_{M=\pm 1/2}\left[\frac{|G^0_{c_M}|^2}{\Gamma_{a_M a_M}\left(d_1+\frac{|G^0_{d_M}|^2}{d_3}\right)}\left(\frac{G^0_{p_M}}{d_1}+\frac{G'^0_{p_M}}{d_2}\right)\right.\\ &\left.+\frac{(G^0_{c_M})^* G^0_{d_M}}{d_3\left(d_2+\frac{|(G^0_{d_M})^*|^2}{\Gamma_{a_M a_M}}+\frac{|G^-_{c_M}|^2+|G^+_{c_M}|^2}{d_3}\right)}\times\left(\frac{G^0_{p_M}}{d_2}+\frac{G'^0_{p_M}}{d_4}\right)\right]\\ &-i\sum_{M=\pm 1/2}\frac{1}{\Gamma_{a_M a_M}}\left(\frac{(G^-_{c_M})^* G^-_{c_M}}{d_{13}+\frac{|G^0_{d_M}|^2}{d_3}}+\frac{(G^+_{c_M})^* G^+_{c_M}}{d_{12}+\frac{|G^0_{d_M}|^2}{d_3}}\right)\\ &\times\left(\frac{G^0_{p_M}}{d_1}+\frac{G'^0_{p_M}}{d_2}\right), \end{aligned} \quad (7)$$

$$\begin{aligned}\rho_{P(\mathrm{PMT2})}^{k_1,k_1'} = &-i\sum_{M=\pm 1/2}\frac{|G^0_{d_M}|^2}{\Gamma_{a_M a_M}\left(d_2+\frac{|G^-_{c_M}|^2+|G^+_{c_M}|^2}{d_5}\right)}\left(\frac{G^0_{p_M}}{d_1}+\frac{G'^0_{p_M}}{d_2}\right)\\ &-i\sum_{M=\pm 1/2}\frac{G^0_{c_M}(G^0_{d_M})^*}{d_5\left(d_1+\frac{|(G^-_{c_M})^*|^2+|(G^+_{c_M})^*|^2}{\Gamma_{a_M a_M}}+\frac{|G^0_{d_M}|^2}{d_5}\right)}\\ &\times\left(\frac{G^0_{p_M}}{d_6}+\frac{G'^0_{p_M}}{d_1}\right). \end{aligned} \quad (8)$$

According to Eqs. (5)–(8), the dressing FWM signals can be modulated via the polarizations of the incident laser beams. Simultaneously, the dressing effects also depend on the frequency detuning Δ_1 and Δ_2. Suppression and enhancement derived from the dressing effect can be obtained by adjusting the detuning difference $\Delta(\Delta = \Delta_1 - \Delta_2)$ of the input laser beams [16].

4. RESULTS AND DISCUSSION

In order to observe the intensity and the dressing effect of each FWM signal, we set Δ_2 at $-0.3\,\mathrm{cm}^{-1}$ and scan the detuning Δ_1. Figures 3(a) and 3(b) give the undressed-FWM and $\mathbf{k}_d'$ dressed-FWM signals that are detected by PMT1. With the changing of Δ_1, an emission peak can be observed in each FWM curve. We can see that the degenerate-FWM (DFWM) signal $\mathbf{k}_{s1}$ (normalized intensity $I_1 = 1$) is much stronger than the three nondegenerate-FWM (NDFWM) signals (relative intensities are $I_2 = 0.15 \pm 0.05$, $I_3 = 0.11 \pm 0.04$, and $I_4 = 0.02 \pm 0.006$), and shows a dip at the resonance position $\Delta_1 = 0$. This is attributed to the resonance absorption of the FWM signal. When the dressing field $\mathbf{k}_d'$ is opened, the left peak of signal $\mathbf{k}_{s1}$ is suppressed and the right one is enhanced. On the same condition, other FWM signals are all suppressed. Figures 3(c) and 3(d) give the coexisting FWM signals $\mathbf{k}_{s1} + \mathbf{k}_{s2}$ and $\mathbf{k}_{s3} + \mathbf{k}_{s4}$, respectively. Compared with that of the single FWM signal $\mathbf{k}_{s1}$, the intensity of the coexisting signal $\mathbf{k}_{s1} + \mathbf{k}_{s2}$ is decreased due to the mutual-dressing effect. When another dressing field $\mathbf{k}_d'$ is turned on, the coexisting signal is further suppressed.

Next, we investigate the interactions among these coexisting FWM signals by modifying the polarizations of the incident fields. Based on the results of Fig. 3, we set Δ_2 at $-0.3\,\mathrm{cm}^{-1}$, Δ_1 at $-0.4\,\mathrm{cm}^{-1}$, and detect the P-polarized FWM components (Figs. 4 and 5). In this case, four FWM signals can be observed simultaneously and the suppressed condition $\Delta_1/m - \Delta_2 = 0$ is satisfied, where m is the modified factor.

Figure 4 shows the dependence of the coexisting FWM signal intensity on the rotation angle θ of the HWP, which is set on the path of the laser beam $\mathbf{k}_c'$, while other beams keep horizontal polarization. Figures 4(a) and 4(b) give the FWM signals detected by PMT1. There are four coexisting FWM signals, namely, $\mathbf{k}_{s1}$, $\mathbf{k}_{s2}$, $\mathbf{k}_{s3}$, and $\mathbf{k}_{s4}$. Beam $\mathbf{k}_c'$ acts as the coupling field for these FWM signals. The dependence of these FWM intensities on θ follows $(\cos 2\theta)^2$ [10]. In order to explore the interactions among these FWM signals, a different laser beam is blocked in each case. We can see in Fig. 4(a) that the total signal intensity decreases when field $\mathbf{k}_c$ is turned off, but increases when field $\mathbf{k}_d$ is off. In fact, the coupling field $\mathbf{k}_c$ of signals $\mathbf{k}_{s1}$ and $\mathbf{k}_{s3}$ acts as a dressing field for signals $\mathbf{k}_{s2}$

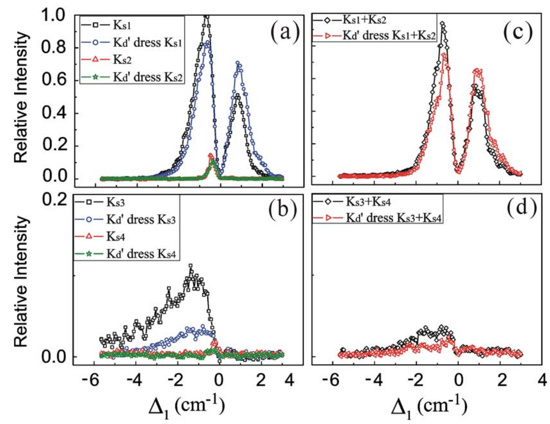

Fig. 3. (Color online) Relative intensities of four FWM signals ($\mathbf{k}_{s1}$, $\mathbf{k}_{s2}$, $\mathbf{k}_{s3}$, $\mathbf{k}_{s4}$) versus Δ_1 with $\Delta_2 = -0.3\,\mathrm{cm}^{-1}$. (a) Undressed-FWM signals $\mathbf{k}_{s1}$, $\mathbf{k}_{s2}$, and $\mathbf{k}_d'$-dressed $\mathbf{k}_{s1}$, $\mathbf{k}_{s2}$. (b) Undressed-FWM signals $\mathbf{k}_{s3}$, $\mathbf{k}_{s4}$, and $\mathbf{k}_d'$-dressed $\mathbf{k}_{s3}$, $\mathbf{k}_{s4}$. (c) Coexisting FWM signals $\mathbf{k}_{s1} + \mathbf{k}_{s2}$ and $\mathbf{k}_d'$-dressed $\mathbf{k}_{s1} + \mathbf{k}_{s2}$. (d) Coexisting FWM signals $\mathbf{k}_{s3} + \mathbf{k}_{s4}$ and $\mathbf{k}_d'$-dressed $\mathbf{k}_{s3} + \mathbf{k}_{s4}$.

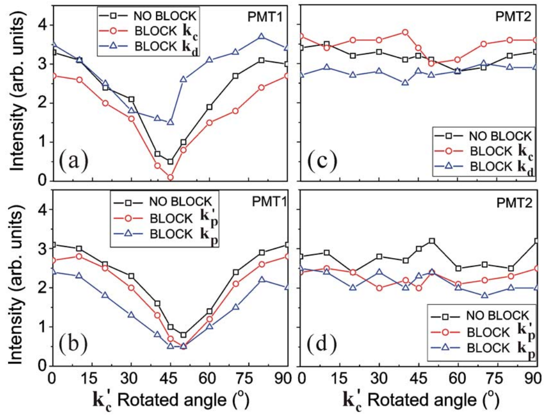

Fig. 4. (Color online) Dependence of the FWM signal intensity on the rotation angle of the HWP put on the path of field $\mathbf{k}'_c$. (a)–(c) FWM signals when coupling field $\mathbf{k}_c$ or $\mathbf{k}_d$ is blocked. Squares, six laser beams are all turned on; circles, $\mathbf{k}_c$ is blocked; triangles, $\mathbf{k}_d$ is blocked. (b)–(d) FWM signals when probe field $\mathbf{k}_p$ or $\mathbf{k}'_p$ is blocked. Squares, six laser beams are all turned on; circles, $\mathbf{k}'_p$ is blocked; triangles, $\mathbf{k}_p$ is blocked.

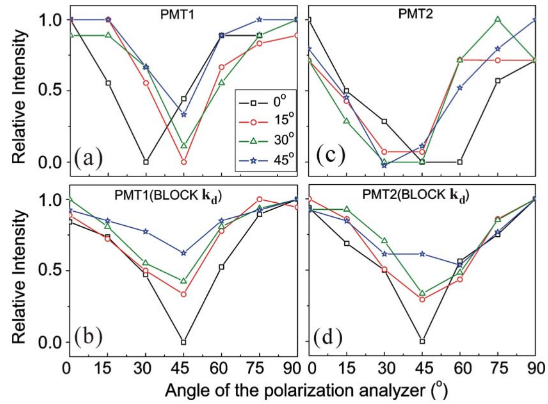

Fig. 5. (Color online) Dependence of the relative FWM signal intensity on the rotation angle of the polarization analyzer for four values of the ellipticity of field $\mathbf{k}_c$. (a)–(c) FWM signals detected by PMT1 and PMT2, respectively. (b)–(d) FWM signals detected by PMT1 and PMT2 when $\mathbf{k}_d$ is blocked. Squares, $\theta = 0°$ (θ is the polarization angle of $\mathbf{k}_c$); circles, $\theta = 15°$; triangles, $\theta = 30°$; asterisks, $\theta = 45°$.

and $\mathbf{k}_{s4}$. When field $\mathbf{k}_c$ is blocked, FWM signals $\mathbf{k}_{s1}$ and $\mathbf{k}_{s3}$ disappear, but FWM signals $\mathbf{k}_{s2}$ and $\mathbf{k}_{s4}$ become stronger because of the absence of the suppression effect of the dressing field. However, as mentioned above, DFWM signal $\mathbf{k}_{s1}$ is much stronger than NDFWM signals, so the total intensity decreases. On the contrary, when field $\mathbf{k}_d$ is blocked, the total signal intensity increases. Figure 4(b) shows the cases of blocking probe fields $\mathbf{k}_p$ and $\mathbf{k}'_p$. In these two cases, the total signal intensities are all decreased. This is because signals $\mathbf{k}_{s1}$ and $\mathbf{k}_{s2}$ (or $\mathbf{k}_{s3}$ and $\mathbf{k}_{s4}$) disappear when $\mathbf{k}_p$ (or $\mathbf{k}'_p$) blocked, but the dressing field does not change. The different phenomenon in each case clearly shows the mutual dressings among coexisting FWM signals. For the signals detected by PMT2, field $\mathbf{k}'_c$ acts as a dressing field. The signal intensities show little change with rotation angle θ in Figs. 4(c) and 4(d). This means the polarization direction of the FWM signals depends mainly on the coupling field. The total signal intensity detected by PMT2 increases when field $\mathbf{k}_c$ is turned off, but decreases when field $\mathbf{k}_d$ is off. The result also can be explained by the mutual-dressing effect of coexisting FWM signals.

Then, we measure the ellipticity of the coexisting FWM signals. A QWP was used to modulate the ellipticity of incident field $\mathbf{k}_c$. In order to detect the polarization states of the FWM signals, a special combination HWP + PBS is used as a polarization analyzer put on the path of the FWM signals. Figure 5 illustrates the dependence of the relative FWM signal intensity on the rotation angle of the polarization analyzer. We can see in Figs. 5(a) and 5(b) that the oscillation amplitudes of the signals in PMT1 change with the ellipticity of $\mathbf{k}_c$, and this change becomes more obvious when $\mathbf{k}_d$ is blocked (only $\mathbf{k}_{s1}$ and $\mathbf{k}_{s3}$ exist). As mentioned above, $\mathbf{k}_c$ is the coupling field for signals $\mathbf{k}_{s1}$ and $\mathbf{k}_{s3}$. When $\mathbf{k}_c$ is rotated from $\theta = 0°$ to $\theta = 45°$, the polarizations of $\mathbf{k}_{s1}$ and $\mathbf{k}_{s3}$ change from linear polarization to elliptic polarization [10], thus the oscillation amplitudes of $\mathbf{k}_{s1}$ and $\mathbf{k}_{s3}$ clearly decrease. However, the polarizations and the oscillation amplitudes of signals $\mathbf{k}_{s2}$ and $\mathbf{k}_{s4}$ do not change under the polarization rotation of dressing field $\mathbf{k}_c$. Therefore, there is not remarkable decrease in the oscillation amplitude at $\theta = 45°$ when the four FWM signals coexist. For the signals detected by PMT2, field $\mathbf{k}_c$acts mainly as a dressing field. The curves exhibit little sensitivity to the ellipticity of $\mathbf{k}_c$ [as shown in Fig. 5(c)]. However, when $\mathbf{k}_d$ is blocked, the oscillation amplitude changes with the ellipticity of $\mathbf{k}_c$. These results mean the ellipticity of the FWM signals is determined mainly by the coupling field, while the polarization states of the dressing field show little influence on the ellipticity of the FWM signals.

Now we investigate the polarization dependence of the dressing strength of the FWM signals. The polarization of the dressing field stays linearly polarized and the ellipticity of the coupling field (and the FWM signals) is changed by the QWP. To show different dressing effects, we set Δ_1 at different values and scan Δ_2.

First, when Δ_1 is set at a small value (the suppressed condition $\Delta_1/m - \Delta_2 = 0$ is satisfied), FWM signals are suppressed by the dressing field. Figure 6 shows the polarization dependence of the suppressed FWM signals in PMT1 when probe field $\mathbf{k}'_p$ is blocked and coupling field $\mathbf{k}_c$ is modulated

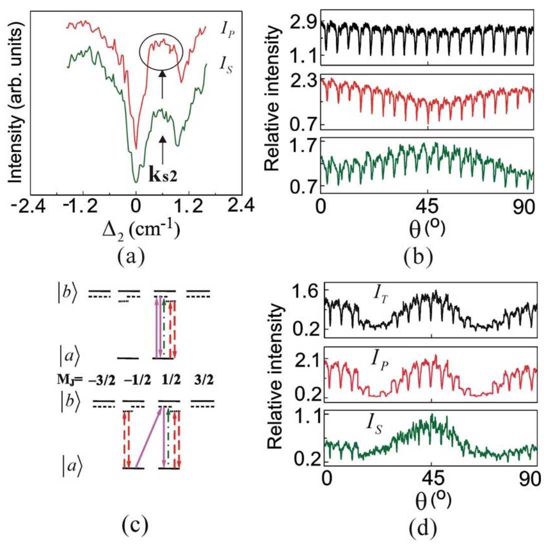

Fig. 6. (Color online) Polarization dependence of the suppression of FWM signals versus the rotation angle of the QWP. (a) FWM signals when $\mathbf{k}_c$ is at 45°. (b) Field $\mathbf{k}_c$ is modulated by the QWP. (c) Zeeman sublevel schemes. (d) Fields $\mathbf{k}_c$ and $\mathbf{k}'_c$ are simultaneously modulated by the QWP.

by QWP. Figure 6(a) gives one curve detected at 45°. In such case there are two FWM signals, $\mathbf{k}_{s1}$ and $\mathbf{k}_{s2}$, dressed by $\mathbf{k}_d$ and $\mathbf{k}'_d$. With the detuning Δ_2 scanned, NDFWM signal $\mathbf{k}_{s2}$ presents an emission peak at $\Delta_2 = \Delta_1$, and DFWM signal $\mathbf{k}_{s1}$ presents a suppression dip at $\Delta_2 = \Delta_1/m$. Figure 6(b) shows the curves detected at different polarization angles (from 0° to 90° per 5°). The background represents the signal intensity of the FWM without a dressing field, while the dips represent that the signal was suppressed by the dressing field. We can see that the suppression dips become deeper when the polarization angle is rotated from 0° to 45°. Such a phenomenon indicates that the dressing field has different dressing strengths for FWM signals with different ellipticity. The result can be explained by the mutual-dressing effect. As discussed above, the DFWM signal $\mathbf{k}_{s1}$ can be generated through two balanced transition subsystems:

$$|a_{1/2}\rangle \xrightarrow{G^0_{c2}} |b_{1/2}\rangle \xrightarrow{G'^0_{c2}} |a_{1/2}\rangle \xrightarrow{G^0_{p2}} |b_{1/2}\rangle \xrightarrow{(G^0_{F2})^*} |a_{1/2}\rangle,$$

$$|a_{-1/2}\rangle \xrightarrow{G^0_{c1}} |b_{-1/2}\rangle \xrightarrow{G'^0_{c1}} |a_{-1/2}\rangle \xrightarrow{G'^0_{p1}} |b_{-1/2}\rangle \xrightarrow{(G^0_{F1})^*} |a_{-1/2}\rangle,$$

when $\theta = 0°$. Figure 6(c) shows the former transition pathway. If only the mutual-dressing effect is considered, the corresponding density matrix element of the signal $\mathbf{k}_{s1}$ can be expressed as

$$\rho_1^{k_1} = \frac{-iG^0_{p2}G^0_{c2}(G^0_{c2})^*}{\Gamma_{a_{1/2}a_{1/2}}\left(i\Delta_1 + \Gamma_{b_{1/2}a_{1/2}} + \frac{|G^0_{d2}|^2}{i(\Delta_1-\Delta_2)+\Gamma_{a_{1/2}a_{1/2}}}\right)(i\Delta_1 + \Gamma_{b_{1/2}a_{1/2}})}. \tag{9}$$

When $\theta = 45°$, the two transition pathways generating the signal $\mathbf{k}_{s1}$ are

$$|a_{-1/2}\rangle \xrightarrow{G^+_{c1}} |b_{1/2}\rangle \xrightarrow{G'^0_{c2}} |a_{1/2}\rangle \xrightarrow{G^0_{p2}} |b_{1/2}\rangle \xrightarrow{(G^+_{F2})^*} |a_{1/2}\rangle,$$

$$|a_{1/2}\rangle \xrightarrow{G^-_{c2}} |b_{-1/2}\rangle \xrightarrow{G'^0_{c1}} |a_{-1/2}\rangle \xrightarrow{G^0_{p1}} |b_{-1/2}\rangle \xrightarrow{(G^-_{F1})^*} |a_{-1/2}\rangle.$$

Figure 6(c) also shows the first transition pathway. The corresponding density matrix element can be written as

$$\rho_5^{k_1} = \frac{-iG^0_{p2}G^+_{c1}(G^0_{c2})^*}{\Gamma_{a_{1/2}a_{1/2}}\left(i\Delta_1 + \Gamma_{b_{1/2}a_{-1/2}} + \frac{|G^0_{d2}|^2}{i(\Delta_1-\Delta_2)+\Gamma_{a_{-1/2}a_{-1/2}}}\right)^2}. \tag{10}$$

Comparing the denominator of Eq. (9) with that of Eq. (10), the dressing term $|G^0_{d2}|^2/[i(\Delta_1 - \Delta_2) + \Gamma_{a_{\pm1/2}a_{\pm1/2}}]$ exists one time in Eq. (9), but it is quadratic in Eq. (10). We can conclude that the FWM signal is dressed one time by G_d at 0°, while it is dressed two times by G_d at 45°. So the dressing efficiency at 45° is higher than that at 0°.

Figure 6(d) presents the experimental results when the polarizations of fields $\mathbf{k}_c$ and $\mathbf{k}'_c$ are changed simultaneously by the QWP. In this case, the background curve obeys the formula $I_P \propto I(\sin^4\theta + \cos^4\theta)[\sin^4(\theta+\theta_0) + \cos^4(\theta+\theta_0)]$, where θ_0 is the polarization angle difference between $\mathbf{k}_c$ and $\mathbf{k}'_c$. The period of the curve is $\pi/4$ [17]. Field $\mathbf{k}'_c$ is set at a 45° polarization angle before field $\mathbf{k}_c$ ($\theta_0 = 45°$). When the rotation angle of the QWP is at $\theta = 0°$, the polarization angle of field $\mathbf{k}_c$ is at 0°, and that of $\mathbf{k}'_c$ is at 45°. According to their transition pathways (see Table 2) and Eq. (10), the FWM signal is dressed two times by G_d. When the QWP is rotated to $\theta = 45°$, field $\mathbf{k}_c$ is at 45° polarization, and field $\mathbf{k}'_c$ is at 90° polarization. The FWM signal also is dressed two times by G_d. Therefore, the largest suppression dips are at both $\theta = 0°$ and $\theta = 45°$.

Second, when the frequency detuning Δ_1 gets larger, the enhancement condition ($\Delta_1/m - \Delta_2 + G_d = 0$) is satisfied. Figure 7(a) gives the variations of the enhancement peaks versus the polarization angle of field $\mathbf{k}_c$. The enhancement peak is strongly heightened at $\theta = 0°$, but lower clearly at $\theta = 45°$. As discussed above, when field $\mathbf{k}_c$ is rotated from 0° to 45°, the polarization of the DFWM signal $\mathbf{k}_{s1}$ changes from linear to elliptic polarization, but the NDFWM signal $\mathbf{k}_{s2}$ stays linearly polarized. In order to show the polarization dependence of the NDFWM signal $\mathbf{k}_{s2}$, field $\mathbf{k}_c$ is blocked and $\mathbf{k}_d$ is modulated by the QWP [as shown in Fig. 7(b)]. Signal $\mathbf{k}_{s2}$ shows an emission peak and its intensity changes with the polarization of coupling field $\mathbf{k}_d$. However, because DFWM signal $\mathbf{k}_{s1}$ is much stronger than NDFWM signal $\mathbf{k}_{s2}$, the Fig. 7(a) presents mainly the variation of the enhancement peak height of $\mathbf{k}_{s1}$. Such a variation can be explained by the self-dressing effect. On the condition of far detuning, both the mutual-dressing effect and the self-dressing effect should be considered. So Eqs. (9) and (10) are corrected into

$$\rho_1^{k_1} = \frac{-iG^0_{p2}G^0_{c2}(G^0_{c2})^*}{\Gamma_{a_{1/2}a_{1/2}}\left(i\Delta_1 + \Gamma_{b_{1/2}a_{1/2}} + \frac{|G^0_{d2}|^2}{i(\Delta_1-\Delta_2)+\Gamma_{a_{1/2}a_{1/2}}} + \frac{|G^0_{c2}|^2}{\Gamma_{a_{1/2}a_{1/2}}}\right)(i\Delta_1 + \Gamma_{b_{1/2}a_{1/2}})}, \tag{11}$$

$$\rho_5^{k_1} = \frac{-iG^0_{p2}G^+_{c1}(G^0_{c2})^*}{\Gamma_{a_{1/2}a_{1/2}}\left(i\Delta_1 + \Gamma_{b_{1/2}a_{-1/2}} + \frac{|G^0_{c1}|^2}{\Gamma_{a_{-1/2}a_{-1/2}}} + \frac{|(G^0_{c1})^+|^2}{\Gamma_{a_{-1/2}a_{-1/2}} + \frac{|G^0_{d2}|^2}{i(-\Delta_2)+\Gamma_{a_{-1/2}b_{-1/2}}}} + \frac{|G^0_{d2}|^2}{i(\Delta_1-\Delta_2)+\Gamma_{a_{-1/2}a_{-1/2}}}\right)^2}. \tag{12}$$

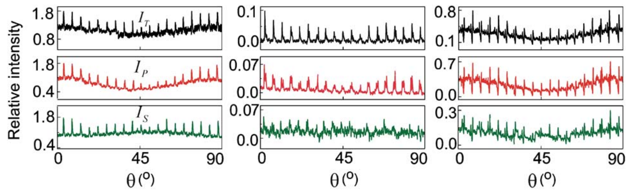

Fig. 7. (Color online) Polarization dependence of the enhancement of FWM signals versus the rotation angle of the QWP. (a) Field $\mathbf{k}_c$ is modulated by the QWP. (b) Field $\mathbf{k}_c$ is blocked, and $\mathbf{k}_d$ is modulated by the QWP. (c) Field $\mathbf{k}'_c$ is modulated by the QWP.

From Eqs. (11) and (12) we can see that, when Δ_1 becomes large enough, the value of $|G^0_{d2}|^2/[i(\Delta_1 - \Delta_2) + \Gamma_{a_{\pm1/2}a_{\pm1/2}}]$ decreases and, thus, the mutual-dressing efficiency of G_d decreases, and self-dressing field G_c plays a dominant role. Since the CG coefficients can be different for different transitions between Zeeman sublevels, if considering multiplied CG coefficients of each transition pathway [12], we can obtain that the Rabi frequency of the self-dressing field G_c at 45° is smaller than that at 0°, so the self-dressing efficiency at 45° is less than that at 0°.

Finally, when frequency detuning Δ_1 is adjusted at an intermediate value, the FWM signals show half-enhancement and half-suppression [as shown in Fig. 7(c)]. The dependences of the suppression dips and enhancement peaks on the polarization are similar to the results obtained under the pure-enhancement condition. This indicates that the self-dressing effect also plays an important role in this case.

5. CONCLUSION

In summary, the dependences of eight coexisting FWM signals in a two-level atomic system on the polarization configurations are investigated. The intensities of coexisting FWM signals depend both on the polarizations and the frequency detunings of the coupling fields. The mutual-dressing and self-dressing effects present different efficiencies at different detuning conditions and polarization states. It is obtained that the polarization states of the coexisting FWM signals depend mainly on the ellipticities of the coupling fields. These results provide an effective way to control the coexisting FWM signals.

ACKNOWLEDGMENTS

This work was supported by the National Natural Science Foundation of China (NSFC, 10974151, 61078002, 61078020, 11104214, 611108017, 11104216), the New Century Excellent Talent Project of the Ministry of Education of China (NCET, 08-0431), the Specialized Research Fund for the Doctoral Program of Higher Education of China (RFDP, 20100201120031), and the Cross-Disciplinary Project of Xi'an Jiaotong University (2009xjtujc08, xjj20100100, xjj20100151).

REFERENCES

1. P. B. Chapple, K. G. H. Baldwin, and H. A. Bachor, "Interference between competing quantum-mechanical pathways for four-wave mixing," J. Opt. Soc. Am. B **6**, 180 (1989).
2. W. C. Magno, R. B. Prandini, P. Nussenzveig, and S. S. Vianna, "Four-wave mixing with Rydberg levels in rubidium vapor: observation of interference fringes," Phys. Rev. A **63**, 063406 (2001).
3. S. W. Du, J. M. Wen, M. H. Rubin, and G. Y. Yin, "Four-wave mixing and biphoton generation in a two-level system," Phys. Rev. Lett. **98**, 053601 (2007).
4. S. W. Du, E. Oh, J. M. Wen, and M. H. Rubin, "Four-wave mixing in three-level systems: interference and entanglement," Phys. Rev. A **76**, 013803 (2007).
5. E. F. McCormack and E. Sarajlic, "Polarization effects in quantum coherences probed by two-color, resonant four-wave mixing in the time domain," Phys. Rev. A **63**, 023406 (2001).
6. K. Tsukiyama, "Parametric four-wave mixing in Kr," J. Phys. B **29**, L345 (1996).
7. L. Museur, C. Olivero, D. Riedel, and M. C. Castex, "Polarization properties of coherent VUV light at 125 nm generated by sum-frequency four-wave mixing in mercury," Appl. Phys. B **70**, 499–503 (2000).
8. J. Ishii, Y. Ogi, Y. Tanaka, and K. Tsukiyama, "Observation of the two-photon resonant parametric four-wave mixing in the NO $C^2\Pi(v=0)$ state," Opt. Commun. **132**, 316–320 (1996).
9. C. J. Zhu, A. A. Senin, Z. H. Lu, J. Gao, Y. Xiao, and J. G. Eden, "Polarization of signal wave radiation generated by parametric four-wave mixing in rubidium vapor: ultrafast (~150 fs) and nanosecond time scale excitation," Phys. Rev. A **72**, 023811 (2005).
10. R. M. Wang, Y. G. Du, Y. P. Zhang, H. B. Zheng, Z. Q. Nie, C. B. Li, Y. Y. Li, J. P. Song, and M. Xiao, "Polarization spectroscopy of dressed four-wave mixing in a three-level atomic system," J. Opt. Soc. Am. B **26**, 1710–1719 (2009).
11. H. B. Zheng, Y. P. Zhang, U. Khadka, R. M. Wang, C. B. Li, Z. Q. Nie, and M. Xiao, "Modulating the multi-wave mixing processes via the polarizable dark states," Opt. Express **17**, 15468–15480 (2009).
12. C. B. Li, Y. P. Zhang, Z. Q. Nie, Y. G. Du, R. M. Wang, J. P. Song, and M. Xiao, "Controlling enhancement and suppression of four-wave mixing via polarized light," Phys. Rev. A **81**, 033801 (2010).
13. Z. Q. Nie, H. B. Zheng, P. Z. Li, Y. M. Yang, Y. P. Zhang, and M. Xiao, "Interacting multiwave mixing in a five-level atomic system," Phys. Rev. A **77**, 063829 (2008).
14. Y. P. Zhang and M. Xiao, "Generalized dressed and doubly-dressed multiwave mixing," Opt. Express **15**, 7182–7189 (2007).
15. C. B. Li, Y. P. Zhang, Z. Q. Nie, H. B. Zheng, C. C. Zuo, Y. G. Du, J. P. Song, K. Q. Lu, and C. L. Gan, "Controlled multi-wave mixing via interacting dark states in a five-level system," Opt. Commun. **283**, 2918–2928 (2010).
16. C. B. Li, H. B. Zheng, Y. P. Zhang, Z. Q. Nie, J. P. Song, and M. Xiao, "Observation of enhancement and suppression in four-wave mixing processes," Appl. Phys. Lett. **95**, 041103 (2009).
17. Y. P. Zhang, C. C. Zuo, H. B. Zheng, C. B. Li, Z. Q. Nie, J. P. Song, H. Chang, and M. Xiao, "Controlled spatial beam splitter using four-wave-mixing images," Phys. Rev. A **80**, 055804 (2009).